Control Engineering Practice 151 (2024) 106038

Contents lists available at ScienceDirect

Control Engineering Practice

journal homepage: www.elsevier.com/locate/conengprac

Linear active disturbance rejection control for large onshore wind turbines in full wind speed range☆

Chengzhen Jia [a,*], Hua Geng [a], Yushan Liu [b], Lingmei Wang [b,*], Enlong Meng [b], Jiwen Ji [b], Zhengkun Chen [b], Lei Han [b], Liming Chen [c], Dongjie Guo [d], Jiye Liang [e], Yinping Fenghong [f]

[a] Department of Automation, Tsinghua University, No. 1 Qinghuayuan Haidian District, Beijing, 100084, China
[b] Institute of Green Energy and Electric Power Intelligent Control, Shanxi University, No. 63 Nanzhonghuan East Street, Xiaodian District, Taiyuan, 030006, China
[c] School of Computing, Ulster University, 2-24 York Street, Belfast, BT15 1AP, United Kingdom
[d] SPIC Shanxi new energy Co., Ltd, No. 705 Changfeng Street, Taiyuan, 030006, China
[e] School of Computer and Information Technology, Shanxi University, No. 92 Wucheng Street, Taiyuan, 030006, China
[f] School of Mathematical Sciences, Shanxi University, No. 92 Wucheng Street, Taiyuan, 030006, China

ARTICLE INFO

Keywords:
Anti-interference
Torque control
Pitch control
One-order LADRC
Generator rotor speed
Load force

ABSTRACT

To achieve real-time estimation and compensation of total system disturbances and improve the control performance of wind turbines under complex turbulent wind conditions, three one-order LADRCs were used to reconstruct the wind turbine core control system. A dynamic variable limit LADRC was designed for torque control, a minimum limit LADRC was applied in pitch control, and a LADRC power controller was designed for decoupling torque and pitch control. The stability of the LADRCs was proven using the Lyapunov method. According to the transfer function of wind turbines and empirical equations, the parameters of each LADRC were tuned. Based on the hardware-in-loop simulation (HILS) test platform, the control algorithm of look-up table, PID, RISC, and LADRC were constructed by PLC language. Through comparative studies, it was verified that the algorithm proposed in this paper can reduce generator rotor speed and power fluctuations by about 13.6% and 1.7% at least, and it can also reduce the blade root load force.

1. Introduction

"Carbon neutrality" is the global consensus, and vigorously developing renewable energy such as wind power is one of the effective ways to achieve this goal. With the development of large-scale wind turbines, the flexibility of wind turbine towers and blades has become increasingly apparent, and their dynamic characteristics have become increasingly complicated under turbulent wind conditions (Byrne, Hewitt, Griffiths, et al., 2021; Liu, Lei, Yang, et al., 2021; Wang, Cai, Xu et al., 2021). Furthermore, large-scale onshore wind turbines are highly susceptible to unpredictable disturbances due to turbulent wind conditions, making it challenging to establish precise mathematical models. The ability to withstand disturbances not only impacts control performance, but also has a significant impact on the load of wind turbine components, the large load can significantly reduce the lifespan of the components, and in extreme cases, it can even pose a risk of the wind turbine tipping over. This places heightened demands on the anti-interference controls of large-scale wind turbines. To achieve safe, stable, and efficient control of wind turbines, it is essential to estimate and compensate for uncertain system disturbances and implement model-free self-disturbance rejection control techniques.

In recent years, scholars have done a lot of research on wind turbine control, mainly focusing on the following two aspects: torque control and pitch control. The basic DTU wind energy controller applicable for pitch-regulated, variable speed wind turbines is reported, and the PID control method is adopted (Civelek, Çam, Luy, et al., 2016; Hansen & Henriksen, 2013), it has been used in 10 MW complex nonlinear wind turbine model. Fig. 1 shows the diagram of the DTU wind energy controller. Due to the error feedback mechanism of PID control strategy, its ability to combat interference is limited. An adaptive control based on radial basis function neural network(RBFNN) is proposed including torque control, pitch control and smooth transition between the two control loop, the RBF NN control is robust to uncertainty in the wind

☆ This document is the results of the research project funded by the National Natural Science Foundation of China (No. 62303261), Key R&D Plan Projects in Shanxi Province (No. 202202060301004, No. 202202010101001), Shanxi Province Special Project for Science and Technology Cooperation and Exchange (No. 202104041101020) and Transformation of Scientific and Technological Achievements Guiding Special Project of Shanxi Province (No. 202204021301064).

* Corresponding authors.
E-mail addresses: m18856452899@163.com (C. Jia), 13546468676@163.com (L. Wang).

https://doi.org/10.1016/j.conengprac.2024.106038
Received 31 January 2024; Received in revised form 2 July 2024; Accepted 1 August 2024
Available online 8 August 2024

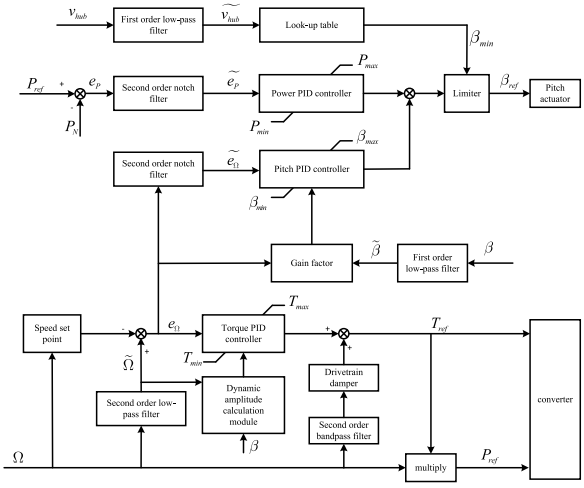

Fig. 1. Diagram of the DTU wind energy controller.

turbine model (Jafarnejadsani, Pieper, & Ehlers, 2013), however, to ensure effective control, it is crucial to train the RBFNN in advance, as the training accuracy significantly impacts the control outcome. Below the rated wind speed, the wind turbine achieves the maximum wind energy utilization by controlling the electromagnetic torque (Zhou, Yin, Yang, et al., 2021). In order to overcome the uncertain disturbance of the system, the sliding mode torque control method is adopted (Mahnoosh, Seyed, Saeed, et al., 2020; Oscar, Jose, Isidro, et al., 2019), but eliminating the chatting is a challenge for the application of sliding mode control(SMC). A ℓ_1 controller is used to minimize the effect of persistent disturbances in wind turbine systems (Jafarnejadsani & Pieper, 2015), a NMPC controller is used to maximize the energy capture and minimize the torque fluctuation of the generator simultaneously (Song, Tu, Wang, et al., 2022; Soued, Ebrahim, Ramadan, et al., 2017), but these model-based controller has high computational complexity and the control effect is limited by the accuracy of the system model. Above the rated wind speed, the wind turbine maintains constant speed and power of the generator through pitch control. An inverse system control (ISC) method is proposed for power control of variable pitch wind power systems, however, it is imperative to devise robust compensation methods to enhance the disturbance rejection capability of ISC (Geng, Zhou, & Yang, 2010). For power regulation, an adaptive second order SMC is applied to the nonlinear system as wind turbine, and significantly enhance the pitch control accuracy and compensate for model uncertainties and external disturbances (Yin, Zhang, Jiang, et al., 2019; Zhang & Plestan, 2021), but it is also facing the defect of dead zone oscillation on the sliding mode surface. Fractional order proportional integral and derivative (FOPID) controller is used for pitch angle control (Halil, 2021), but it is sensitive to system disturbances and has poor robustness. Based on the soft measurement of wind speed, a feedforward and feedback variable rotor controller is designed (Pan, Xiong, Zhu, et al., 2022), and a composite pitch control strategy is designed by using lidar wind measurement data, which further reduces the power and speed fluctuation, and increases the anti-interference performance of the control system (Jia, Wang, Meng, et al., 2021), but, forward control places stringent demands on the system model, any discrepancies in the system model can result in a deterioration of the anti-interference performance.

Based on the aforementioned research, it is evident that the control of wind turbines is primarily categorized into two methods: model-free control and model-based control. Model-free control techniques, such as PI, FOPID, SMC, RBFNN are employed, while model-based control techniques, such as NMPC, ℓ_1, ISC, are also utilized. The PI control needs to cooperate with different filters, such as low-pass filter, bandpass filter, notch filter, and so forth. PI control has limitations in anti-interference. NMPC, ℓ_1 and RBFNN are restricted by PLC computation, and they are not easily implemented in engineering applications. Additionally, SMC is prone to chattering on the sliding mode surface. In conclusion, a new algorithm is necessary that takes into account advantages related to model-free, ease of engineering implementation, and avoidance of filtering processes.

At present, some scholars have applied ADRC to the converter control (Beltran-Pulido, Cortes-Romero, & Coral-Enriquez, 2018; Li, Zhang, Li, et al., 2016) and pitch control (Coral-Enriquez, Cortes-Romero, & Dorado-Rojas, 2019) of wind turbine. However, there has been no previous report on the LADRC strategy simultaneously applied to torque-speed loop and pitch-speed loop control in full wind speed range. LADRC is model-free, and it views internal and external disturbances as the total disturbance of the system, and estimates the disturbance in real time through the ESO (Wu, Li, Liu, et al., 2023; Wu, Sui, Li, et al., 2024), making it suitable for addressing the control challenges of nonlinear and strongly coupled wind turbine systems. The main contributions and novelties of this paper to the existing literature are as follows:

(1) The torque-speed loop and pitch-speed loop is reconstructed by using first-order LADRC. A dynamic variable limit first-order LADRC is utilized to achieve unified torque control in the minimum rotor speed section, variable rotor speed section, and maximum rotor speed section. A minimum limit LADRC was applied in pitch control. A LADRC power controller for decoupling torque and pitch control.

(2) The response characteristics of the closed-loop system are compared and analyzed using the Bode diagram analysis method. It is demonstrated that the LADRC eliminates the need for complex filtering links and partially simplifies the core control structure. Additionally, the LADRC is straightforward to implement in practical engineering scenarios.

(3) By comparing different control algorithms, the experimental results show that the LADRC strategy has advantages in reducing the power, generator rotor speed fluctuations, and it can also reduce the blade root load force.

Therefore, it is of great significance to use three LADRCs to design the torque and pitch control loop and investigate its impact on wind turbines. The main contents include the following aspects. In Section 2, the mathematical model of the wind turbine is analyzed in detail. In Section 3, the control loop of wind turbines based on LADRCs is designed. The parameters of LADRC are tuned based on the transfer function of wind turbine and empirical equations in Section 4. In Section 5, a HILS test platform based on Matlab/Simulink, FAST and Beckhoff PLC is established, and case studies and analysis are carried out on the test platform. The last section concludes this work.

2. The model of DTU 10 MW wind turbine

The establishment of the multi-body dynamic model for the DTU 10 MW wind turbine was achieved using FAST v8.16. The hub height of the wind turbine is 119 m, while the rotor diameter is 183.9 m. The first flap frequency of the blade is 0.61 Hz, the first edge frequency is 0.93 Hz, and the first fore-aft and side-side mode frequency of the tower is 0.25 Hz (Bak, Zahle, Bitsche, et al., 2013). The Cp curve for the wind turbine is shown in Fig. 2. Cp represents the wind energy capture efficiency. The operation of a wind turbine is a highly complex and nonlinear process.

If the drive train is modeled as a rigid shaft and the external damping coefficients of the wind turbine and generator are ignored, the dynamic characteristics of the drive train can be represented by a first-order differential equation (Ren, Mao, Song, et al., 2019; Zhang, Wei, Xu, et al., 2021; Zouheyr, Lotfi, & Abdelmadjid, 2021).

$$\begin{cases} T_{\text{aero}} = \frac{1}{2}\rho\pi R^3 v^2 C_{\text{T}}(\lambda,\beta) \\ \left(J_{\text{r}} + n_{\text{g}}^2 J_{\text{g}}\right)\dot{\Omega} = T_{\text{aero}} - n_{\text{g}} T_{\text{em}} \end{cases} \tag{1}$$

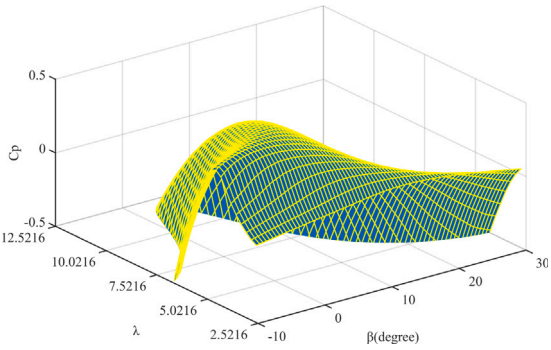

Fig. 2. Wind turbine Cp schematic.

where, ρ is air density, R is impeller radius, υ is wind speed, C_T is torque coefficient, λ is tip speed ratio, β is pitch angle, J_r and J_g respectively represent the inertia moment of the rotor and generator, n_g is transformation ratio of the gearbox, T_{em} is the electromagnetic torque of the generator, Ω is the rotor speed, T_{aero} is the pneumatic torque.

Below the rated wind speed, the unit will maintain a constant minimum pitch angle. Typically, the pitch angle is set to 0, and formula (1) can be expressed as Eq. (2).

$$J\dot{\Omega} = f_A(\Omega, \upsilon) - n_g T_{em} \tag{2}$$

In this formula, $J = J_r + n_g^2 J_g$ is the total inertia moment, f_A represents aerodynamic torque below rated wind speed, which is a nonlinear function of Ω and υ.

At wind speeds exceeding the rated wind speed, the electromagnetic torque T_{em} of the unit remains constant, and the rotor speed is maintained at the rated value by adjusting the pitch angle. The Eq. (3) is got.

$$J\dot{\Omega} = f_B(\Omega, \upsilon, \beta) - n_g T_{em} \tag{3}$$

In formula (3), f_B represents aerodynamic torque above the rated wind speed. The formula (3) can reflect the dynamic characteristics of generator speed varying with pitch angle, while the pitch actuator dynamics can be equivalent to Eq. (4) (Bak et al., 2013).

$$\beta_B = \frac{bs+1}{a^2 s^2 + bs + 1}\beta_r \tag{4}$$

In formula (4), $a = \frac{1}{\omega_0}$, $b = \frac{2\zeta}{\omega_0}$, ζ is damping rate of pitch system, ω_0 is natural frequency of pitch system, β_r represents the change of the pitch angle command, β_B represents the change of the pitch angle.

The generator rotor speed of the wind turbine varies in response to changes in wind speed within the impeller plane. Fig. 3 illustrates the torque-speed control curve, with the green line representing the dual PI control curve and the yellow line denoting the lookup table control curve. This is the most critical and core curve in wind turbine control. In region 1, the rotor speed reaches the minimum grid-connected speed, and torque increases linearly while maintaining a constant speed. In region 2, the unit operates according to the optimal blade-tip speed ratio. In region 3, the unit has reached the rated rotor speed, and torque increases linearly with a constant speed until the rated torque is reached. In region 4, constant power control or constant torque control can be adopted. Constant torque control refers to a control strategy aimed at sustaining an unchanging electromagnetic torque value beyond the rated wind speed. On the other hand, constant power control denotes a control strategy focused on sustaining a consistent output power value.

It can be observed from Fig. 3 that there exist two links with fixed slopes in the lookup table control, and the MPPT 1 interval is smaller than the MPPT 2 interval. As a result, the dual PI control curve enhances wind energy utilization. The PI controller is commonly

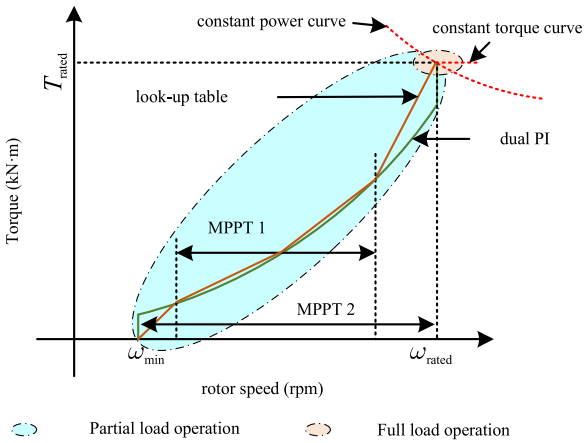

Fig. 3. Wind turbine control curve schematic. (For interpretation of the references to color in this figure legend, the reader is referred to the web version of this article.)

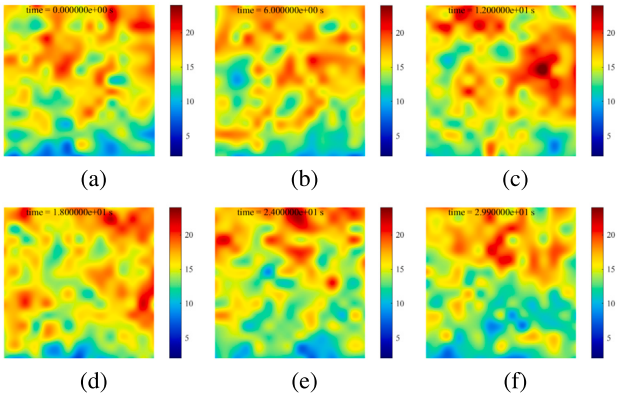

Fig. 4. Wind speed sectional drawing within the range of rotor diameter. (a) t = 0 s; (b) t = 6 s; (c) t = 12 s; (d) t = 18 s; (e) t = 24 s; (f) t = 29.9 s.

implemented in current wind turbines. By using generator rotor speed error feedback as the controller's input, the disturbances in the system are not effectively mitigated. Given the limitations of the PID control algorithm, torque-pitch control of wind turbines is rebuilt using three LADRCs.

The main external disturbance faced by wind turbines is wind. We use TurbSim to generate the turbulent wind files required for simulation. Fig. 4 shows the wind speed profiles of the impeller plane at different times. The average wind speed is 15 m/s.

Based on Fig. 4, it is evident that the wind speed is incessantly changing, and the wind speed across different regions within the turbine surface varies, and the load on the turbine blades is relatively intricate. Compounded by the nonlinear aerodynamic characteristics of the blades, necessitating a control algorithm with exceptional anti-interference and robustness to ensure the wind turbine's safe and stable operation.

3. Torque and pitch controller design based on LADRC

Compared to Fig. 1, this article presents a novel control architecture comprising three LADRCs, as illustrated in Fig. 5. This architecture includes a torque LADRC controller with dynamic limit values, a pitch LADRC controller and a power LADRC controller with minimum amplitude limitation. By utilizing cabin vibration signals to implement resistance control on the wind turbine, the tower load force fluctuation in the flapwise and edgewise direction can be effectively reduced.

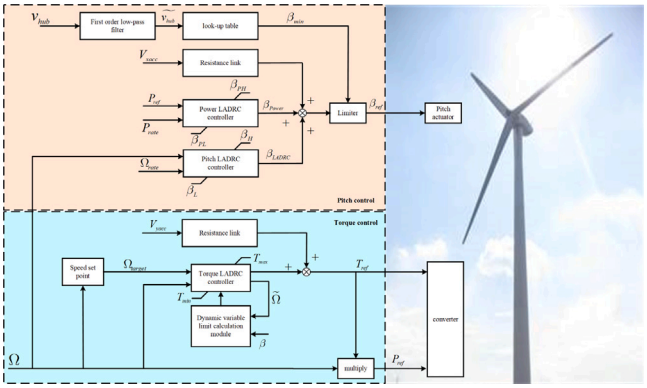

Fig. 5. Diagram of wind turbine control algorithm based on LADRC.

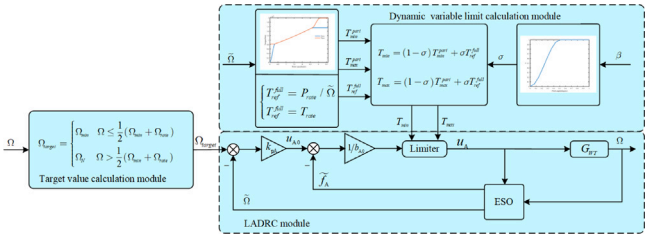

Fig. 6. Dynamic variable limit one-order LADRC of torque controller.

The hub-height wind speed is represented by v_{hub}. $\widetilde{v_{\text{hub}}}$ denotes the filtered wind speed, $\beta_{\min}$ stands for the minimum pitch angle. P_{ref} and P_{rate} represent the command value of power and the rated power value, respectively. β_{PH} and β_{PL} are the maximum and minimum values of the power LADRC controller. β_{Power} denotes the output pitch angle command of the power LADRC controller. Ω_{rate} represents the rated rotor speed. β_{L} and β_{H} are the maximum and minimum values of the pitch LADRC controller. β_{LADRC} denotes the output pitch angle command of pitch LADRC controller. β and β_{ref} represents the pitch angle and pitch angle command value, respectively. Ω_{target} represents the rotor speed target value, T_{ref} denotes the electromagnetic torque command value. $T_{\min}$ and $T_{\max}$ are the maximum and minimum values of the torque LADRC controller. $\widetilde{\Omega}$ is the estimated rotor speed. V_{xacc} and V_{yacc} denote the vibration values in the x and y directions of the cabin.

3.1. Dynamic variable limit LADRC of torque controller

Based on the dynamic characteristics of the torque-speed loop, a one-order LADRC with dynamic variable limit is utilized to achieve unified control of the minimum, variable, and maximum rotor speed sections. The controller block diagram is shown in Fig. 6.

In Fig. 6, u_{A0} is the output of the proportional controller, G_{WT} is the transfer function between torque and rotor speed, $\widetilde{\Omega}$ and $\widetilde{f_{\text{A}}}$ represent the estimation of rotor speed and the total disturbance respectively. ESO is the state observer of first-order LADRC, u_{A} represents the control quantity of electromagnetic torque, and k_{PA} is the proportional parameter, b_{A0} is the given non-zero constant.

According to β and $\widetilde{\Omega}$, the dynamic Ω_{target}, the $T_{\min}$ and $T_{\max}$ value of the first-order LADRC is calculated. The calculation method is as follows: when Ω is not greater than $(\Omega_{\min}+\Omega_{\text{rate}})/2$, and Ω_{target} remains at the minimum value, $\Omega_{\text{target}}=\Omega_{\min}$, the maximum output limit is $k\widetilde{\Omega}^2$, k represents the optimal torque coefficient, and the minimum output limit is 0. When Ω is greater than $(\Omega_{\min}+\Omega_{\text{rate}})/2$, and $\Omega_{\text{target}}=\Omega_{\text{rate}}$, the maximum output limit is $P_{\text{rate}}/\widetilde{\Omega}$, and the minimum output is $k\widetilde{\Omega}^2$. When Ω is greater than $(\Omega_{\min}+\Omega_{\text{rated}})/2$, and β is not the minimum value, $\Omega_{\text{target}}=\Omega_{\text{rate}}$, in case of constant power control, the maximum and minimum output is $P_{\text{rate}}/\widetilde{\Omega}$, in case of constant torque control, the maximum and minimum output is T_{rate}.

When the generator speed is close to its bounds, these torque limits will open according to the interpolation factor, the calculation formula for interpolation factor is as follows (Hansen & Henriksen, 2013).

$$\sigma\left(x_0,x_1;x\right)=\begin{cases}0 & \forall x<x_0\\ a_3x^3+a_2x^2+a_1x+a_0 & \forall x\in[x_0,x_1]\\ 1 & \text{otherwise}\end{cases} \tag{5}$$

Calculation of coefficients in Eq. (5) is as follows.

$$\begin{aligned}a_3&=\frac{2}{\left(x_0-x_1\right)^3}\\ a_2&=\frac{-3\left(x_0+x_1\right)}{\left(x_0-x_1\right)^3}\\ a_1&=\frac{6x_1x_0}{\left(x_0-x_1\right)^3}\\ a_0&=\frac{\left(x_0-3x_1\right)x_0^2}{\left(x_0-x_1\right)^3}\end{aligned}. \tag{6}$$

The minimum generator speed is 300 rpm and rated generator speed is 480 rpm of the DTU 10 MW wind turbine. The limits are set to be closed approximately 5% above the minimum speed and start opening again at 90% and are fully open at 95% of the rated speed. The switching between partial and full load control of the generator torque is based on a first order low-pass filtered switching variable σ that is driven by Eq. (5) evaluation using the measured mean pitch angle β. The time constant is the rotational period at rated speed.

The torque control law is designed as Eq. (7).

$$u_{\text{A}}=\frac{u_{\text{A0}}-z_{\text{A2}}}{b_{\text{A0}}} \tag{7}$$

In Eq. (7), $z_{\text{A2}}\approx\widetilde{f_A}$. After the total disturbance compensation, the system can be regarded as an integral object, so a proportional controller is designed for control, as shown in Eq. (8).

$$\Delta\dot{\Omega}_{\text{A}}\approx u_{\text{A0}}=k_{\text{pA}}\left(\Omega_{\text{target}}-z_{\text{A1}}\right) \tag{8}$$

In Eq. (8), $z_{\text{A1}}\approx\widetilde{\Omega_{\text{A}}}$.

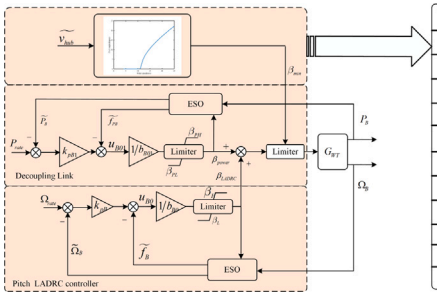

Wind speed (m/s)	Pitch angle (deg)	Wind speed (m/s)	Pitch angle (deg)
4	0	15	10.591
5	0	16	12.042
6	0	17	13.376
7	0	18	14.63
8	0	19	15.824
9	0	20	16.968
10	0	21	18.071
11	0	22	19.141
12	4.507	23	20.181
13	7.088	24	21.192
14	8.991	25	22.175

Fig. 7. The one-order LADRC of pitch controller diagram.

3.2. Pitch LADRC controller with minimum limit

At wind speeds exceeding the rated speed, the dynamic relationship between the pitch angle and rotor speed is represented by Eq. (3). Recognizing that the system's dynamic characteristics become nonlinear at varying wind speeds, LADRC controllers were designed and implemented to enhance the disturbance rejection of the pitch control. The structure of this controller is depicted in Fig. 7.

In Fig. 7, two LADRCs provide β_{LADRC} and β_{power} pitch angle control commands. After passing through a one-order low-pass filter, the

minimum required pitch angle value $\beta_{\min}$ at different wind speed is determined by the nonlinear relationship between wind speed and pitch angle. G_{WT} represents the single input multiple output wind turbine model, $\widetilde{\Omega_B}$ and $\widetilde{f_B}$ represent the estimation of generator speed and disturbance, respectively. ESO is the state observer of one-order LADRC, u_{B0} and u_{B01} represent the control quantity of the pitch angle, and its calculation method is shown in Eq. (7). k_{pB} and k_{pB1} are the proportional parameters, while b_{B0} and b_{B01} are given non-zero constant.

When the wind speed fluctuates near the rated speed, the control objective of the torque and pitch LADRC controllers is to maintain constant generator rotor speed, but the adjustment methods are different, one is to adjust the torque, and the other is to adjust the pitch angle. Therefore, when the wind speed fluctuates near the rated speed, two LADRC controllers will activate simultaneously, resulting in significant fluctuations in power and rotor speed. The decoupling of torque control and pitch control is achieved using a power LADRC controller as shown in Fig. 7. By optimizing the amplitude of the power LADRC controller, it can be guaranteed that the pitch angle remains at the lowest possible value when the generator has not reached its maximum capacity. Once the unit reaches its maximum power, the pitch angle commences its operation while maintaining the torque controller's power command consistent.

3.3. Control stability analysis

Eqs. (2) and (3) are converted into the state space form as follows:

$$\begin{cases} \dot{x}_1 = x_2 + b_0 u \\ \dot{x}_2 = \dot{f}\,(y,d) \\ y = x_1 \end{cases} \tag{9}$$

where, f represents the differential of the system total disturbance, and d represents the external disturbance. The ESO of the system is in the following form:

$$\begin{cases} \dot{z}_1 = z_2 + L_1\,(y - \hat{y}) + b_0 u \\ \dot{z}_2 = L_2\,(y - \hat{y}) + \dot{f}\,(\hat{y}, d) \\ \hat{y} = z_1 \end{cases} \tag{10}$$

Compared with the standard state space expression form, each coefficient matrix in the equation is as follows: $\boldsymbol{A} = \begin{bmatrix} 0 & 1 \\ 0 & 0 \end{bmatrix}$, $\boldsymbol{B} = \begin{bmatrix} b_0 \\ 0 \end{bmatrix}$, $\boldsymbol{C} = \begin{bmatrix} 1 & 0 \end{bmatrix}$, $\boldsymbol{L} = \begin{bmatrix} L_1 \\ L_2 \end{bmatrix} = \begin{bmatrix} 2w_{\mathrm{o}} \\ w_{\mathrm{o}}^2 \end{bmatrix}$, $\boldsymbol{E} = \begin{bmatrix} 0 \\ 1 \end{bmatrix}$, The double poles of the observer are located at w_{o}.

For physical control systems, the generator speed is constrained by mechanical stress limitations, as is the rate of generator speed change. The magnitude and fluctuation of the principal external disturbance wind speed are also bounded. Thus, we can proceed with the following assumptions.

Assuming $\dot{f}(y,d)$ complies with the Lipschitz continuity condition within the given domain, there is a constant, denoted as k, such that $\left|\dot{f}(y,d) - \dot{f}(\hat{y},d)\right| \leq k \parallel y - \hat{y} \parallel$(Chen, Wang, Sun, et al., 2018).

A subtracting by combining Eq. (9) and Eq. (10) is made, let $\varepsilon_1 = x_1 - z_1$, $\varepsilon_2 = \frac{x_2 - z_2}{w_{\mathrm{o}}}$, and Eq. (11) is got.

$$\begin{bmatrix} \dot{\varepsilon}_1 \\ \dot{\varepsilon}_2 \end{bmatrix} = w_{\mathrm{o}} \begin{bmatrix} -2 & 1 \\ -1 & 0 \end{bmatrix} \begin{bmatrix} \varepsilon_1 \\ \varepsilon_2 \end{bmatrix} + \begin{bmatrix} 0 \\ 1 \end{bmatrix} \frac{\dot{f}\,(y,d) - \dot{f}\,(\hat{y},d)}{w_{\mathrm{o}}} \tag{11}$$

let $\boldsymbol{A}_0 = \begin{bmatrix} -2 & 1 \\ -1 & 0 \end{bmatrix}$, $\boldsymbol{B}_0 = \begin{bmatrix} 0 \\ 1 \end{bmatrix}$, through the analysis of the characteristic equation of the system, $\boldsymbol{A}_0$ is Horwitz stable, then there is a positive definite Hermitian matrix $\boldsymbol{P}$, and make a satisfy $\boldsymbol{A}_0^{\mathrm{T}}\boldsymbol{P} + \boldsymbol{P}\boldsymbol{A}_0 = -\boldsymbol{I}$, $\boldsymbol{P} = \begin{bmatrix} \frac{1}{2} & -\frac{1}{2} \\ -\frac{1}{2} & \frac{3}{2} \end{bmatrix}$.

Construct the Lyapunov function $\mathbf{V}(\varepsilon) = \varepsilon^{\mathrm{T}}\boldsymbol{P}\varepsilon$, then,

$$\dot{\mathbf{V}}(\varepsilon) = -w_{\mathrm{o}}\left(\varepsilon_1^2 + \varepsilon_2^2\right) + \frac{\dot{f}\,(y,d) - \dot{f}\,(\hat{y},d)}{w_{\mathrm{o}}}\left(-\varepsilon_1 + 3\varepsilon_2\right) \tag{12}$$

According to Lipschitz continuity condition,

$$\frac{\dot{f}(y,d) - \dot{f}(\hat{y},d)}{w_{\mathrm{o}}}(-\varepsilon_1 + 3\varepsilon_2) \leqslant k(-\varepsilon_1 + 3\varepsilon_2)\frac{\parallel y - \hat{y} \parallel}{w_{\mathrm{o}}}. \tag{13}$$

And because $-\varepsilon_1 + 3\varepsilon_2 = 2\varepsilon^{\mathrm{T}}\boldsymbol{P}\boldsymbol{B}_0$, Eq. (13) can be transformed into,

$$2\varepsilon^{\mathrm{T}}\boldsymbol{P}\boldsymbol{B}_0\frac{\dot{f}(y,d) - \dot{f}(\hat{y},d)}{w_{\mathrm{o}}} \leqslant 2k\varepsilon^{\mathrm{T}}\boldsymbol{P}\boldsymbol{B}_0\frac{\parallel y - \hat{y} \parallel}{w_{\mathrm{o}}} \tag{14}$$

When $w_{\mathrm{o}} \geq 1$, there is $\frac{\|y-\hat{y}\|}{w_{\mathrm{o}}} = \frac{\|\varepsilon\|}{w_{\mathrm{o}}} \leqslant \| \varepsilon \|$. Meanwhile, due to $\| \boldsymbol{P}\boldsymbol{B}_0 k \|^2 - 2 \| \boldsymbol{P}\boldsymbol{B}_0 k \| + 1 \geqslant 0$, we can get,

$$\dot{\mathbf{V}}(\varepsilon) \leq -w_{\mathrm{o}}\left(\varepsilon_1^2 + \varepsilon_2^2\right) + \left(\left\|\boldsymbol{P}\boldsymbol{B}_0 k\right\|^2 + 1\right)\|\boldsymbol{\varepsilon}\|^2 \tag{15}$$

From Eqs. (12) and (15), it can be concluded that,

$$\dot{\mathbf{V}}(\varepsilon) = -w_{\mathrm{o}}\left(\varepsilon_1^2 + \varepsilon_2^2\right) + \left(\|\boldsymbol{P}\boldsymbol{B}_0 k\|^2 + 1\right)\varepsilon^2 \tag{16}$$

When $w_{\mathrm{o}} > \left\|\boldsymbol{P}\boldsymbol{B}_0 k\right\|^2 + 1$, $\dot{\mathbf{V}}(\varepsilon) < 0$, according to the conditions of Lyapunov asymptotic stability, there are,

$$\lim_{t\to\infty} x_i(t) - z_i(t) = 0, \quad i = 1, 2 \tag{17}$$

The system error $e = r - y$, combined with the control law Eq. (6) of the one-order LADRC, Eq. (18) can be obtained.

$$\dot{\boldsymbol{e}} = \begin{bmatrix} -k_{\mathrm{p}} \end{bmatrix}\boldsymbol{e} + \begin{bmatrix} -k_{\mathrm{p}} & -1 \end{bmatrix}\tilde{y} \tag{18}$$

In Eq. (18), $\tilde{y} = \boldsymbol{x} - \boldsymbol{z}$, k_{p} makes the characteristic polynomial of Eq. (18) satisfy the Routh criterion. At the same time, it can be seen from Eq. (18), $\lim_{t\to\infty} \|e(t)\| = 0$. According to the Lyapunov's asymptotic stability, the first-order LADRC is not only asymptotic stability, but also engineering stability.

4. Parameter tuning of LADRC

Based on Section 3.3, it is evident that LADRC comprises two control parameters: b_0 and w_{o}. To date, numerous studies have been conducted on LADRC parameter tuning. A tuning rule was proposed with the constraint of a specified robustness measure (Wang, Tan and Cui, 2021; Zhang, Tan, & Li, 2019). In this paper, the open-loop transfer function was obtained using the open-loop identification method, which mirrored the dynamic characteristics of the system. By analyzing the open-loop transfer function, an estimation of the value of b_0 was derived. w_{o} was adjusted according to the first-order natural frequency of wind turbines' key components.

4.1. Torque LADRC controller tuning

The open-loop disturbance experiment of torque is carried out for different operating sections under the steady wind speed. The torque step change is 1000 N·m. The transfer function identification of torque-speed link is shown in Fig. 8.

We utilize the Matlab system identification toolbox to fit the transfer functions that can reflect the dynamic characteristics of torque-speed, achieving a fitting accuracy of over 89%. As wind speed increases, the cutoff frequency also increases, indicating that the system's dynamic response speed to external inputs is accelerated. From the identified model, it can be observed that the approximate range of b_{A0} is [0.00018 0.0004]. Based on the first-order frequency of the wind turbine tower, the observation bandwidth w_{Ao} of the ESO can be determined to be 1.256 rad/s. There is a multiple relationship between w_{Ao} and w_{Ac}, approximately $w_{\mathrm{Ac}} = (0 \sim 1)w_{\mathrm{Ao}}$ (Han & Tan, 2021). $w_{\mathrm{Ac}} = 0.5w_{\mathrm{Ao}}$ is taken in this paper.

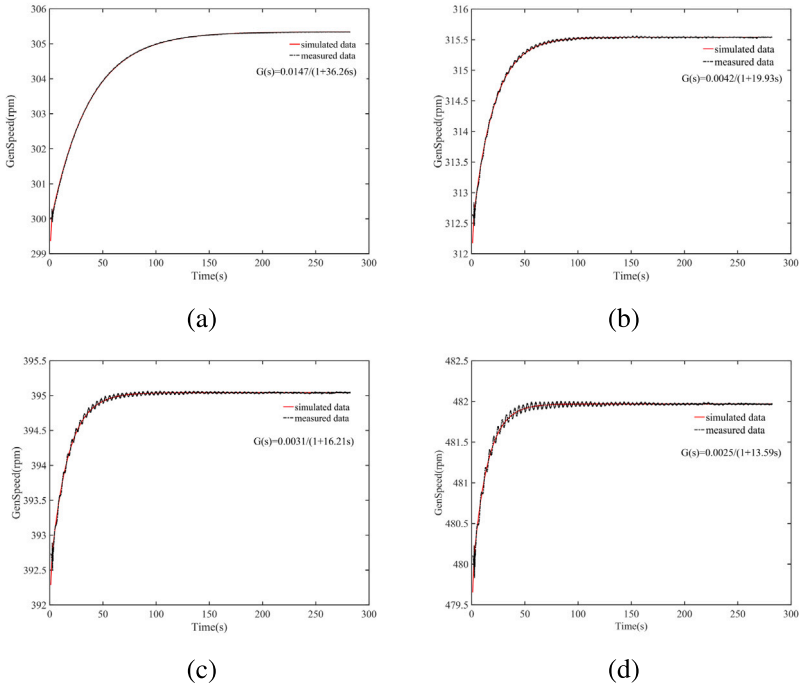

Fig. 8. Identification of torque-speed loop. (a) The wind speed is 5 m/s; (b) The wind speed is 7 m/s; (c) The wind speed is 9 m/s; (d) The wind speed is 11 m/s.

Eq. (19) can be obtained by combining Eqs. (7), (8) and (9).

$$\begin{cases} z_{\mathrm{A1}}(s) = \dfrac{2w_{\mathrm{Ao}}s+w_{\mathrm{Ao}}^2}{(s+w_{\mathrm{Ao}})^2}y(s) + \dfrac{b_{\mathrm{Ao}}s}{(s+w_{\mathrm{Ao}})^2}u_{\mathrm{A}}(s) \\ z_{\mathrm{A2}}(s) = \dfrac{w_{\mathrm{Ao}}^2}{(s+w_{\mathrm{Ao}})^2}sy(s) - \dfrac{b_{\mathrm{Ao}}w_{\mathrm{Ao}}^2}{(s+w_{\mathrm{Ao}})^2}u_{\mathrm{A}}(s) \\ u_{\mathrm{A}}(s) = \dfrac{2w_{\mathrm{Ac}}(r(s)-z_{\mathrm{A1}}(s))-z_{\mathrm{A2}}(s)}{b_{\mathrm{A0}}} \end{cases} \tag{19}$$

Because the controlled object is simplified as a first-order inertial link, the model of the controlled object can be expressed as Eq. (20).

$$y(s) = \frac{\mathrm{K_A}}{\tau s+1}u_{\mathrm{A}}(s) \tag{20}$$

where, $\mathrm{K_A}$ represents the system gain and τ is the inertia time constant of the system. Combining Eqs. (19) and (20), the closed-loop transfer function of the system can be obtained as follows.

$$\begin{cases} G_{\mathrm{clA}}(s) = \dfrac{A_1s^2+A_2s+A_3}{B_1s^3+B_2s^2+B_3s+B_4} \\ A_1 = 2\mathrm{K_A}w_{\mathrm{Ac}} \\ A_2 = 4\mathrm{K_A}w_{\mathrm{Ac}}w_{\mathrm{Ao}} \\ A_3 = 2\mathrm{K_A}w_{\mathrm{Ac}}w_{\mathrm{Ao}}^2 \\ B_1 = b_{\mathrm{A0}}\tau \\ B_2 = 2b_{\mathrm{A0}}\tau w_{\mathrm{Ao}} + 2b_{\mathrm{A0}}\tau w_{\mathrm{Ac}} + b_{\mathrm{A0}} \\ B_3 = 2b_{\mathrm{A0}}w_{\mathrm{Ao}} + 2b_{\mathrm{A0}}w_{\mathrm{Ac}} + \mathrm{K_A}w_{\mathrm{Ao}}^2 + 4\mathrm{K_A}w_{\mathrm{Ac}}w_{\mathrm{Ao}} \\ B_4 = 2\mathrm{K_A}w_{\mathrm{Ac}}w_{\mathrm{Ao}}^2 \end{cases} \tag{21}$$

In the above formula, A_1, A_2, A_3 represent the coefficients of each order of the numerator polynomial, and B_1, B_2, B_3, B_4 represent the coefficients of each order of the denominator polynomial. Take the closed-loop transfer function of the system under different wind speed as an example, w_{Ao} and b_{A0} are tuned, $b_{\mathrm{A0}} = 0.00018$, $w_{\mathrm{Ao}} = 1.256$. The Bode plots are drawn in Fig. 9.

It can be seen from Fig. 9 that the selected parameters can ensure the stable control of the system under different wind. The Bode plots of the closed-loop system characteristic equation is similar to the first-order inertial link, which is consistent with Eq. (8).

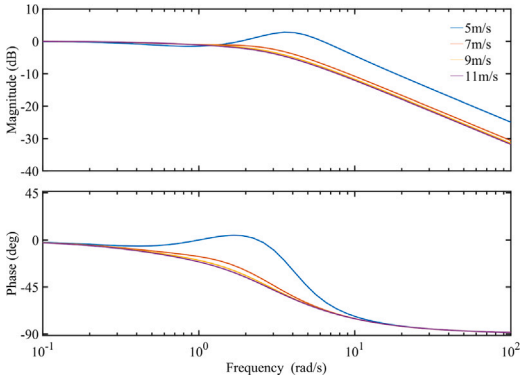

Fig. 9. Bode plots of torque-speed loop.

4.2. Pitch LADRC controller tuning

According to Eq. (3), the dynamic characteristics between speed and pitch angle can be simplified as one order system. The transfer function of the control object is fitted through the open loop pitch angle disturbance experiment, the pitch angle step change is 1 degree, the pitch-speed fitting functions under different wind speeds are shown in Fig. 10, the fitting accuracy is more than 90%.

As we can see from Fig. 10, with the increase of wind speed, the inertia of the system gradually decreases, and the response speed of open-loop system increases. From the identified model, it can be seen that the approximate range of b_{B0} is [307 514]. Based on the first-order frequency of the wind turbine tower, the observation bandwidth w_{Bo} of the ESO can be determined to be 1.256 rad/s. $b_{\mathrm{B0}} = 410$, $w_{\mathrm{Bc}} = 0.1w_{\mathrm{Bo}}$ is taken in this paper. Similarly, using formula (19), (20) and (21), we analyze the bode plots of the pitch-speed closed loop system, as shown in Fig. 11.

From Fig. 11, it can be seen that only one set of LADRC control parameters is needed to achieve stable control of pitch angle above the rated wind speed. So the LADRC control algorithm has strong robustness.

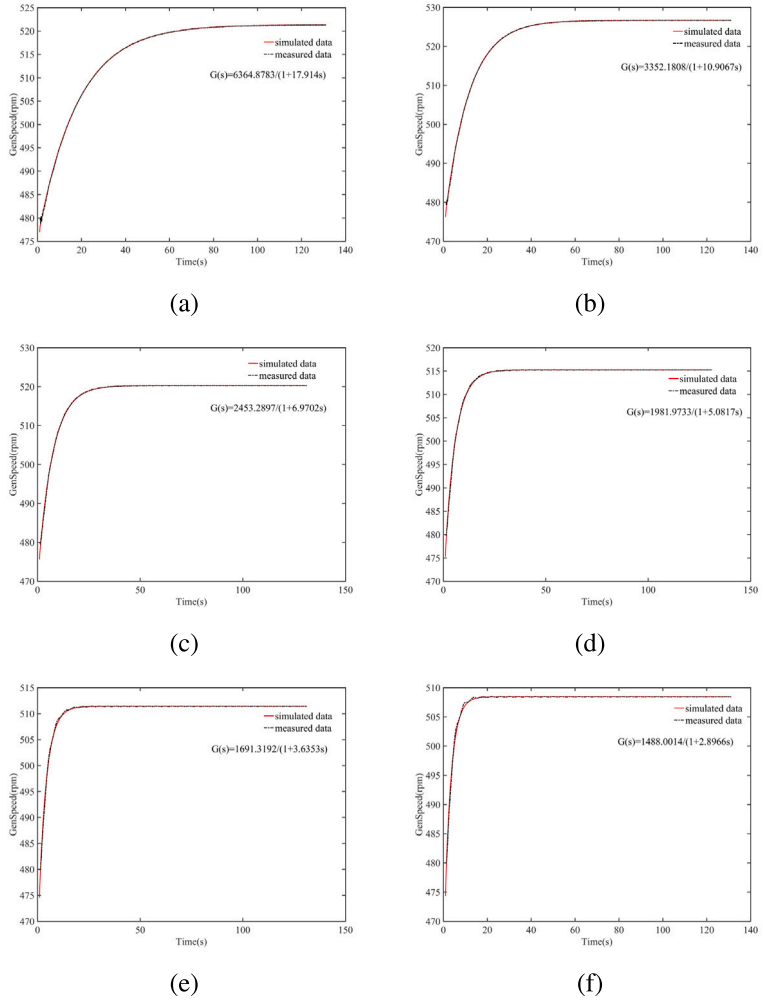

Fig. 10. Identification of pitch-speed loop. (a) The wind speed is 12 m/s; (b) The wind speed is 14 m/s; (c) The wind speed is 16 m/s; (d) The wind speed is 18 m/s; (e) The wind speed is 20 m/s; (f) The wind speed is 22 m/s.

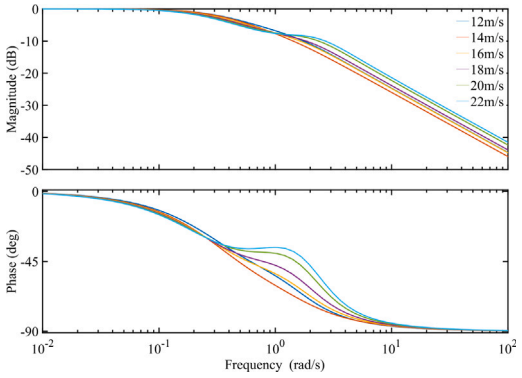

Fig. 11. Bode plots of pitch-speed loop.

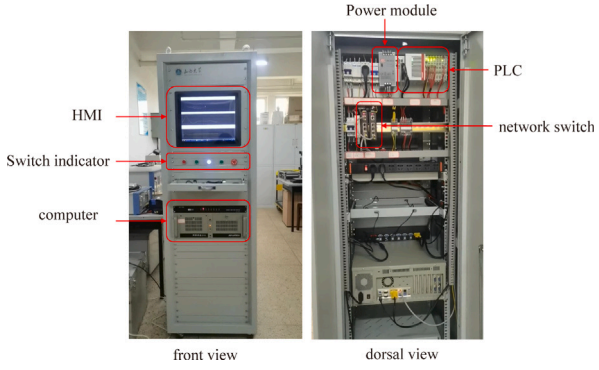

Fig. 12. The physical picture of the test platform.

5. Testing and analysis

5.1. HILS control algorithm test platform

In order to apply the designed control algorithm to practical wind turbine, the HIL test of control algorithm is an essential step. A test and verification platform based on the DTU 10 MW wind turbine model and Beckhoff PLC was built. The platform is built on the open-source software FAST, which was called the model through the s-function interface compiled by FAST v8.16 software. The FAST model contains hundreds of data output interfaces. The algorithms torque-speed control and pitch-speed control were implemented using ST and CFC languages. The exchange of information between the wind turbine model and PLC was achieved through Modbus TCP. The compilation and download of the control algorithm were realized using TwinCAT 3 programming software. The physical picture of the platform is shown in Fig. 12.

In the testing platform, the simulation step of Simulink is 10 ms, and the control cycle of the PLC controller is also 10 ms. Additionally, the

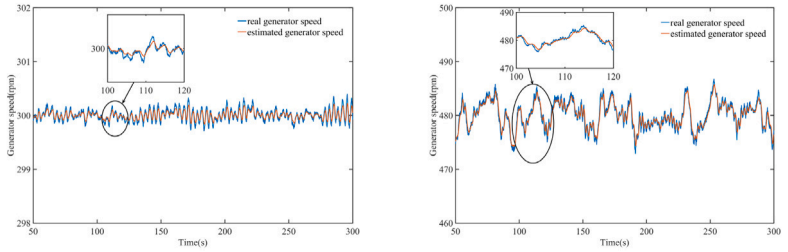

Fig. 13. Observer observation effect. (a) Observation effect of torque controller; (b) Observation effect of pitch controller.

Table 1
10 MW wind turbine parameters.

General properties	Parameters
Cut in wind speed	4 m/s
Cut out wind speed	25 m/s
Rated wind speed	11.2 m/s
Rated power	10 MW
Rotor diameter	178.3 m
Hub diameter	5.6 m
Hub height	119 m
Minimum rotor speed	6 rpm
Maximum rotor speed	9.6 rpm
Gearbox ratio	50
Hub inertia about rotor axis	32 5670.9 kg m^2
Generator inertia about HSS	1500.5 kg m^2

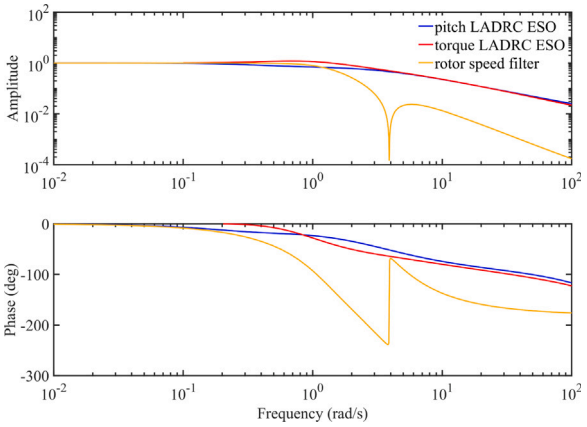

Fig. 14. Bode diagram of different algorithms.

platform facilitates a hardware reset button, making it convenient to restore all system parameters to their initial values. This testing platform can serve as a solid foundation for conducting tests and analyzing cases presented in the following chapter. The design parameters of the 10 MW test wind turbine mentioned in the article are presented in Table 1.

5.2. Tracking effect and bode diagram analysis of LADRC ESO

ESO is the central component of the LADRC controller, and its observation has a direct impact on control effectiveness. The observer's observation effectiveness influences the LADRC control effectiveness. Fig. 13 demonstrates the impact of ESO observation effectiveness on the system under wind speeds of 6 m/s and 12 m/s, with w_o set at 1.256 rad/s.

As shown in Fig. 13, the torque controller and pitch controller demonstrate superior performance in tracking the actual speed across a wide range of wind speeds. By implementing LADRC, the need for low-pass filter in the speed signal is eliminated, enabling direct input into the system. Fig. 14 further displays the bode diagram of generator speed filter and ESO.

Based on the bode diagram, it is evident that the amplitude frequency characteristic of the first-order LADRC ESO closely resembles that of a first-order low-pass filter. However, the generator speed filter displays superior filtering characteristics due to its utilization of a second-order low-pass filter and notch filter. This is an area that requires further improvement in the ESO.

5.3. Control effect under step wind speed

The control algorithms used in the test comparison are shown in Table 2. The control algorithms can be roughly divided into two categories: model-free control methods and model-based control methods. Algorithm 1 (Jonkman, Butterfield, Musial, et al., 2009), algorithm 2 (Lou, Cai, Ye, et al., 2018) and the algorithm proposed in this article is model-free control methods. Algorithm 3 (Geng et al., 2010) is model-based control methods.

In order to analyze the transient characteristics of the control system, the wind speed with step change in different operation intervals was selected. The system dynamic response is shown in Fig. 15.

As can be seen from Fig. 15(a) and (c), compared with algorithm 2 and the proposed algorithm, the rotor speed of algorithm 1 and algorithm 3 control method in the minimum speed area is greater than the minimum speed, while the speed in the maximum speed area is less than the maximum speed, which reduces the wind energy utilization of the wind turbine. In terms of speed control, it can be seen from Fig. 15(a), (c) and (d) that the proposed algorithm has better transient characteristics than algorithm 2. When the wind speed changes, the rotor speed fluctuation of wind turbine with the proposed algorithm is smaller and the rotor speed can reach the stable value faster. In the variable speed area like Fig. 15(b), the control effect of rotor speed is relatively close because both algorithm 1, algorithm 2, algorithm 3 and the proposed algorithm adopt the same control law. In Fig. 15(a), (b), (c) and (d), when the wind speed changes gradually, due to the presence of the tower drag link, the pitch angle is slightly adjusted to reduce flapping vibrations in the tower. In Fig. 15(d), the pitch angle response speed is the fastest using algorithm 3, and the ability to suppress speed fluctuation is strong, the control effect of the proposed algorithm in this paper is the second. However, it is limited to the control effect under steady conditions, and turbulent wind conditions typically exist during wind turbine operation. Section 5.4 will compare the control effects of different control algorithms under turbulent wind conditions.

5.4. Control effect under turbulent wind speed

To approximate actual wind conditions, the TurbSim module in FAST software was employed to simulate three-dimensional turbulent wind. The IECVKM turbulence model was adopted, and the turbulence intensity is 0.05. With turbulent wind conditions having mean values

Table 2
The control algorithms.

Control algorithms	Below rated wind speed	Transition region	Above rated wind speed
Algorithm 1	Look-up table	NaN	GSPID(constant torque)
Algorithm 2	PID	PID	GSPID(constant power)
Algorithm 3	Look-up table	PID	RISC(constant torque)
The proposed algorithm	LADRC	LADRC	LADRC(constant power)

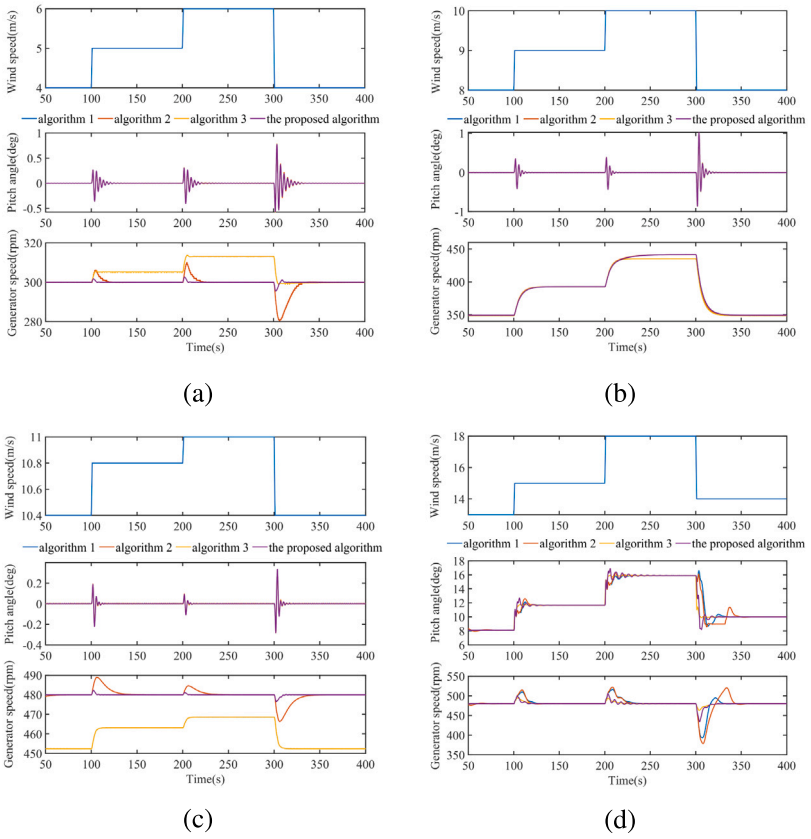

Fig. 15. Comparison of control effects under step wind speed. (a) Minimum speed zone control effect; (b) Variable speed zone control effect; (c) Maximum speed zone control effect; (d) Rated power area control effect.

of 6 m/s, 8 m/s, 10 m/s, 12 m/s, 14 m/s, 16 m/s, 18 m/s, 20 m/s and 22 m/s serving as test examples, the control effects are depicted in Fig. 16.

In Fig. 16, all algorithms can control speed and power stability. In Fig. 16(a), due to differences in control algorithms, algorithms 1 and 3 maintain high speeds, while algorithms 2 and the proposed algorithm maintain speeds near the minimum speed for most of the time. This is because in the minimum speed zone, the control target setting value for algorithm 2 and the proposed algorithm is the minimum speed value, as shown in Fig. 4. The proposed algorithm can better suppress speed fluctuations, with a standard deviation of generator speed of 0.18. By comparison, using the other three control algorithms, the standard deviation of generator speed is 1.28, 1.22 and 1.28, respectively. Similarly, the standard deviation(std) of power is 138.5 when using the proposed algorithm and is approximately 129.98, 145.92 and 130.33 when using the other three algorithms. Algorithm 2 and the proposed algorithm ensure that the wind turbine has a higher mean power value. The average output power is 1424.48 kW for the proposed algorithm compared to approximately 1372.75 kW, 1423.55 kW, and 1372.7 kW for algorithms 1, 2 and 3, respectively. In Fig. 16(b) and (c), when the wind turbine operates in the variable speed area, the control effects of all four strategies are similar and are guided by an optimal control curve. Above rated wind speed, as shown in Fig. 16(d), (e), (f), (g), (h) and (i), compared to the other three algorithms, the proposed control algorithm demonstrates superior performance in limiting speed and power fluctuations, and pitch angle fluctuations are greater when using algorithm 3 compared to other algorithms. In Fig. 16(d), the std of generator speed and power using the proposed algorithm is 5.62 and 63.09, respectively. Under the other three control algorithms, the std of generator speed is 7.74, 11.76, and 4.78, while the power std is 215.46, 96.08 and 121.11. In Fig. 16(e), The std of generator speed and power using the proposed algrithm is 3.43 and 84.77, respectively, under the other three control algorithms, the std of generator speed is 7.05, 8.75, 4.66, the std of power is 201.97, 95.2, 128. In Fig. 16(f), The std of generator speed and power using the proposed algrithm is 3.35 and 103.05, respectively, under the other three control algorithms, the std of generator speed is 7.69, 9.08, 5.23, the std of power is 253.67, 116.96, 166.54. In Fig. 16(g), The std of generator speed and power using the proposed algrithm is 3.52 and 154.69, respectively, under the other three control algorithms, the std of generator speed is 8.43, 9.82, 5.84, the std of power is 313.8, 165.17, 200.96. In Fig. 16(h), The std of generator speed and power using the proposed algrithm is 3.81 and 187.13, respectively, under the other three control algorithms, the std of generator speed is 9.11, 10.39, 6.68, the std of power is 372.64, 204.47, 257.21. In Fig. 16(i), The std of generator speed and power using the proposed algrithm is 4.04 and 217.34, respectively, under the other three control algorithms, the std of generator speed is 9.85, 10.98, 7.26, the std of power is 428.2, 242.3, 308.53. To assess the

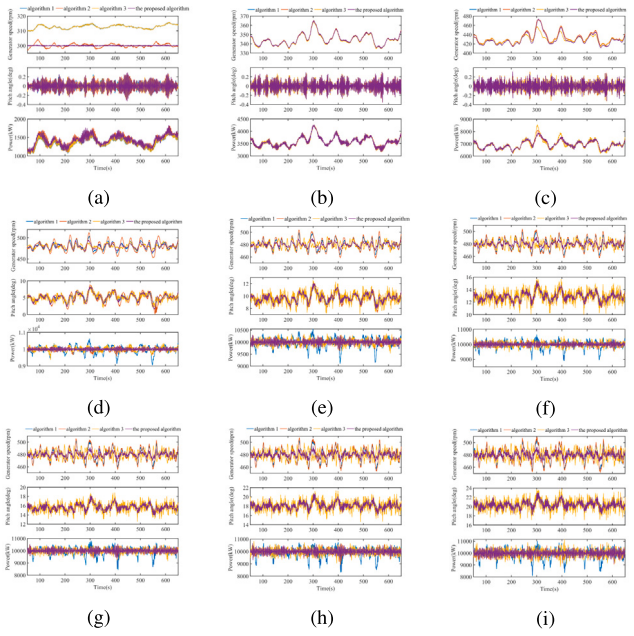

Fig. 16. Comparison of control effects under turbulent wind speed. (a) Turbulent wind with average value of 6 m/s; (b) Turbulent wind with average value of 8 m/s; (c) Turbulent wind with average value of 10 m/s; (d) Turbulent wind with average value of 12 m/s; (e) Turbulent wind with average value of 14 m/s; (f) Turbulent wind with average value of 16 m/s; (g) Turbulent wind with average value of 18 m/s; (h) Turbulent wind with average value of 20 m/s; (i) Turbulent wind with average value of 22 m/s.

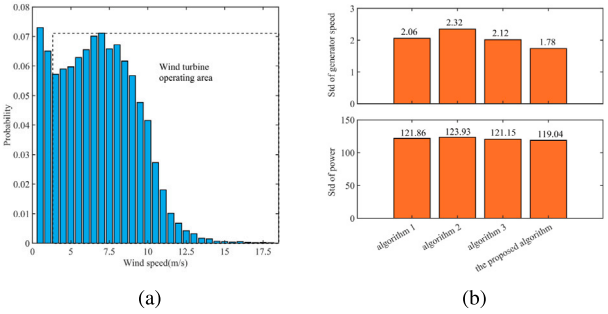

Fig. 17. Comparison of control effects under different control algorithm. (a) Wind speed frequency distribution; (b) Comparison of generator speed and power std.

impact of diverse control algorithms in the entire wind speed range, we conducted a statistical analysis on pertinent metrics, utilizing the wind frequency distribution from the actual wind field, as displayed in Fig. 17.

To verify the control effectiveness of the control algorithm across the entire wind speed range, we multiply the evaluation indicators' values in various wind speed ranges by their corresponding frequency distribution and then sum them up. In Fig. 17(b), it is evident that the control algorithm presented in this article effectively minimizes generator speed and power fluctuations. When compared to algorithm 1, it offers a reduction of 13.6% and 2.3% respectively. When compared to algorithm 2, it offers a reduction of 25.9% and 3.8% respectively. When compared to algorithm 3, it offers a reduction of 16% and 1.7% respectively.

5.5. Comparison of blade root load force

Generally, when we analyze the dynamic load of the wind turbine, the time series length is 10 min, i.e. 600 s. In this part of the test, the

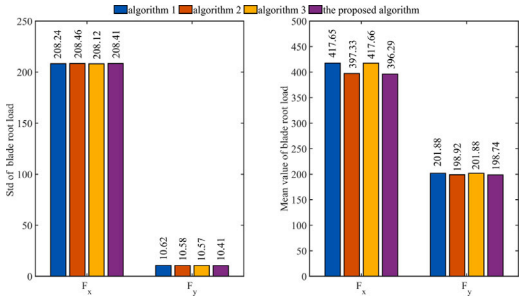

Fig. 18. Comparison of blade root load under different control algorithm.

turbulence wind in Section 5.4 were selected, then the mean and std value of each index were calculated. The impact on blade root load of four different control strategies are compared. The statistical results are shown in Fig. 18.

In Fig. 18, F_x represents the load force in the flapwise direction, and F_y represents the load force in the edgewise direction. It is evident that the proposed algorithm can effectively decrease the mean load force in the flapwise and edgewise direction of blade root, achieving a reduction of 5.1% and 1.5% respectively when compared to algorithm 1 and algorithm 3. Additionally, the proposed algorithm outperforms others in reducing load fluctuation in the edgewise direction of blade root by approximately 1.9%. In the flapwise direction, the load fluctuation of blade root is basically the same.

6. Conclusion

An wind turbine control system based on LADRC has been proposed to obtain satisfactory dynamic characteristics and to reduce the power, generator speed and load force fluctuations. The following conclusions are obtained:

(1) The amplitude frequency characteristics of the one-order LADRC's ESO are comparable to those of a one-order low-pass filter, and it partially simplifies the design of wind turbine control loop. To emulate the characteristics of second-order low-pass filtering and bandpass filtering, an upgrade and enhancement of the ESO structure is necessary.

(2) Particularly above the rated wind speed, the RISC exhibits the fastest response speed in terms of pitch angle, followed closely by LADRC and PID under step wind test conditions. Additionally, the RISC algorithm also displays the strongest ability to mitigate speed fluctuations.

(3) Under turbulent wind conditions, the control algorithm proposed in this article based on LADRC has the best performance in reducing fluctuations in generator speed and power. Simultaneously, it can also minimize the load fluctuations in the edgewise direction of blade root, and it can also reduce the mean value of blade root load.

(4) The upcoming research project aims to integrate ISC and LADRC, leveraging existing model knowledge to optimize the dynamic response characteristics of LADRC pitch control and enhance the overall robustness and interference resistance of the control system.

CRediT authorship contribution statement

Chengzhen Jia: Writing – original draft, Software, Methodology, Formal analysis. **Hua Geng:** Writing – review & editing, Resources, Investigation. **Yushan Liu:** Data curation. **Lingmei Wang:** Project administration. **Enlong Meng:** Funding acquisition. **Jiwen Ji:** Formal analysis, Data curation. **Zhengkun Chen:** Software. **Lei Han:** Methodology, Data curation. **Liming Chen:** Writing – review & editing, Supervision. **Dongjie Guo:** Investigation, Data curation. **Jiye Liang:** Supervision, Software. **Yinping Fenghong:** Formal analysis.

Declaration of competing interest

The authors declare that there are no conflicts of interest in relation to the manuscript. We confirm that the results and interpretations reported in the manuscript are original and have not been plagiarized.

The authors certifies that they have read and understand the Control Engineering Practice conflict of interest policy, and the authors understand that failure to disclose a conflict of interest may result in the manuscript being rejected or retracted.

The authors certifies that they have disclosed any financial or non-financial relationships that may be interpreted as constituting a conflict of interest in relation to this manuscript. The authors understand that this information will be subject to peer review, and they are willing to provide further information or clarification if required.

Acknowledgments

This work was supported by the National Natural Science Foundation of China (No. 62303261), Key R&D Plan Projects in Shanxi Province (No. 202202060301004, No. 2022 02010101001), Shanxi Province Special Project for Science and Technology Cooperation and Exchange (No. 202104041101020) and Transformation of Scientific and Technological Achievements Guiding Special Project of Shanxi Province (No. 202204021301064).

References

Bak, C., Zahle, F., Bitsche, R., et al. (2013). *The DTU 10-MW reference wind turbine: DTU wind energy report-I-0092.*, Denmark: DTU Wind Energy.

Beltran-Pulido, A., Cortes-Romero, J., & Coral-Enriquez, H. (2018). Robust active disturbance rejection control for LVRT capability enhancement of DFIG-based wind turbines. *Control Engineering Practice*, *77*, 174–189. http://dx.doi.org/10.1016/j.conengprac.2018.06.001.

Byrne, R., Hewitt, N. J., Griffiths, P., et al. (2021). Measured wind and morphological characteristics of a peri-urban environment and their impact on the performance of an operational large-scale wind turbine. *Journal of Wind Engineering and Industrial Aerodynamics*, *212*, Article 104592. http://dx.doi.org/10.1016/j.jweia.2021.104592.

Chen, Z., Wang, Y., Sun, M., et al. (2018). Global and asymptotical stability of active disturbance rejection control for second-order nonlinear systems. *Control Theory & Applications*, *35*(11), 1687–1696.

Civelek, Z., Çam, E., Luy, M., et al. (2016). Proportional–integral– derivative parameter optimisation of blade pitch controller in wind turbines by a new intelligent genetic algorithm. *IET Renewable Power Generation*, *10*(8), 1220–1228. http://dx.doi.org/10.1049/iet-rpg.2016.0029.

Coral-Enriquez, H., Cortes-Romero, J., & Dorado-Rojas, S. (2019). Rejection of varying-frequency periodic load disturbances in wind-turbines through active disturbance rejection-based control. *Renewable Energy*, *141*, 217–235. http://dx.doi.org/10.1016/j.renene.2019.04.001.

Geng, H., Zhou, W., & Yang, G. (2010). Inverse-system based robust approach for power control of variable-pitch wind generation system. *Journal of Tsinghua University(Science and Technology)*, *50*(5), 718–723.

Halil, E. (2021). Stability analysis of pitch angle control of large wind turbines with fractional order PID controller. *Sustainable Energy, Grids and Networks*, *26*(6), Article 100430. http://dx.doi.org/10.1016/j.segan.2021.100430.

Han, W., & Tan, W. (2021). Tuning of linear active disturbance rejection controllers based on PID tuning rules. *Control and Decision*, *23*(7), 1592–1600.

Hansen, M. H., & Henriksen, L. C. (2013). *Basic DTU wind energy controller: DTU Wind Energy E No. 0028*, DTU Wind Energy.

Jafarnejadsani, H., & Pieper, J. (2015). Gain-scheduled ℓ_1 -optimal control of variable-speed-variable-pitch wind turbines. *IEEE Transactions on Control Systems Technology*, *23*(1), 372–379. http://dx.doi.org/10.1109/TCST.2014.2320675.

Jafarnejadsani, H., Pieper, J., & Ehlers, J. (2013). Adaptive control of a variable-speed variable-pitch wind turbine using radial-basis function neural network. *IEEE Transactions on Control Systems Technology*, *21*(6), 2264–2272. http://dx.doi.org/10.1109/TCST.2012.2237518.

Jia, C., Wang, L., Meng, E., et al. (2021). Combining LIDAR and LADRC for intelligent pitch control of wind turbines. *Renewable Energy*, *169*, 1091–1105. http://dx.doi.org/10.1016/j.renene.2021.01.065.

Jonkman, J., Butterfield, S., Musial, W., et al. (2009). *Definition of a 5-MW reference wind turbine for offshore system development: NREL/TP-500-38060*, National Renewable Energy Laboratory.

Li, S., Zhang, K., Li, J., et al. (2016). On the rejection of internal and external disturbances in a wind energy conversion system with direct-driven PMSG. *ISA Transactions*, *61*, 95–103. http://dx.doi.org/10.1016/j.isatra.2015.12.014.

Liu, G., Lei, Z., Yang, W., et al. (2021). Mechanism analysis and parameter tuning optimization for wind turbine towers with PS-TMD passive control devices. *Engineering Mechanics*, *38*(12), 137–146. http://dx.doi.org/10.6052/j.issn.1000-4750.2020.11.0851.

Lou, Y., Cai, X., Ye, H., et al. (2018). Optimal generator study based on torque follow-up control for wind turbine. *Transactions of China Electrotechnical Society*, *33*(8), 1884–1893.

Mahnoosh, S., Seyed, K., Saeed, S., et al. (2020). Design of a robust h∞ dynamic sliding mode torque observer for the 100 kW wind turbine. *Sustainable Energy, Grids and Networks*, *24*(12), Article 100393. http://dx.doi.org/10.1016/j.segan.2020.100393.

Oscar, B., Jose, A., Isidro, C., et al. (2019). Variable speed wind turbine control scheme using a robust wind torque estimation. *Renewable Energy*, *133*(4), 354–366. http://dx.doi.org/10.1016/j.renene.2018.10.009.

Pan, L., Xiong, Y., Zhu, Z., et al. (2022). Research on variable pitch control strategy of direct-driven offshore wind turbine using KELM wind speed soft sensor. *Renewable Energy*, *184*, 1002–1017. http://dx.doi.org/10.1016/j.renene.2021.11.104.

Ren, L., Mao, C., Song, Z., et al. (2019). Study on active disturbance rejection control with actuator saturation to reduce the load of a driving chain in wind turbines. *Renewable Energy*, *133*, 268–274. http://dx.doi.org/10.1016/j.renene.2018.10.041.

Song, D., Tu, Y., Wang, L., et al. (2022). Coordinated optimization on energy capture and torque fluctuation of wind turbines via variable weight NMPC with fuzzy regulator. *Applied Energy*, *312*, Article 118821. http://dx.doi.org/10.1016/j.apenergy.2022.118821.

Soued, S., Ebrahim, M. A., Ramadan, H. S., et al. (2017). Optimal blade pitch control for enhancing the dynamic performance of wind power plants via metaheuristic optimisers. *IET Electric Power Applications*, *11*(8), 1432–1440. http://dx.doi.org/10.1049/iet-epa.2017.0214.

Wang, Y., Cai, X., Xu, B., et al. (2021). Study on novel yaw error strategy for wind turbines based on a multi-body dynamics method. *Frontiers in Energy Research*, *9*, Article 711927. http://dx.doi.org/10.3389/fenrg.2021.711927.

Wang, Y., Tan, W., & Cui, W. (2021). Tuning of linear active disturbance rejection controllers for second-order underdamped systems with time delay. *ISA Transactions*, *118*, 83–93. http://dx.doi.org/10.1016/j.isatra.2021.02.011.

Wu, Z., Li, D., Liu, Y., et al. (2023). Performance analysis of improved ADRCs for a class of high-order processes with verification on main steam pressure control. *IEEE Transactions on Industrial Electronics*, *70*(6), 6180–6190. http://dx.doi.org/10.1109/TIE.2022.3192687.

Wu, Z., Sui, S., Li, S., et al. (2024). Modified active disturbance rejection control design based on gain scheduling for selective catalytic reduction denitrification processes. *IEEE Transactions on Industrial Electronics*, *Early Access*, http://dx.doi.org/10.1109/TIE.2024.3387130.

Yin, X., Zhang, W., Jiang, Z., et al. (2019). Adaptive robust integral sliding mode pitch angle control of an electro-hydraulic servo pitch system for wind turbine. *Mechanical Systems and Signal Processing*, *133*, Article 105704. http://dx.doi.org/10.1016/j.ymssp.2018.09.026.

Zhang, C., & Plestan, F. (2021). Individual / collective blade pitch control of floating wind turbine based onadaptive second order sliding mode. *Ocean Engineering*, *228*(5), Article 108897. http://dx.doi.org/10.1016/j.oceaneng.2021.108897.

Zhang, B., Tan, W., & Li, J. (2019). Tuning of linear active disturbance rejection controller with robustness specification. *ISA Transactions*, *85*, 237–246. http://dx.doi.org/10.1016/j.isatra.2018.10.018.

Zhang, S., Wei, J., Xu, Z., et al. (2021). Research on the influence of system parameters on the electromechanical dynamics of a large wind turbine drivetrain. *Energy Reports*, *7*, 7835–7851. http://dx.doi.org/10.1016/j.egyr.2021.11.020.

Zhou, L., Yin, M., Yang, J., et al. (2021). Improved adaptive torque control for wind turbine considering varying turbulence conditions. *Automation of Electric Power Systems*, *45*(1), 184–191.

Zouheyr, D., Lotfi, B., & Abdelmadjid, B. (2021). Improved hardware implementation of a TSR based MPPT algorithm for a low cost connected wind turbine emulator under unbalanced wind speeds. *Energy*, *232*, Article 121039. http://dx.doi.org/10.1016/j.energy.2021.121039.